Eur. Phys. J. D **32**, 51–58 (2005)
DOI: 10.1140/epjd/e2004-00177-0

THE EUROPEAN PHYSICAL JOURNAL D

Analysis of the Fourier transform infrared spectrum of the stannane species $^{116}SnH_4$ in the region 1270–1600 cm^{-1}

A. Tabyaoui[1,2,a], G. Pierre[3], and H. Bürger[4]

[1] L.E.T.S., Faculté des Sciences, avenue Ibn Batouta, B.P. 1014, Rabat, Maroc
[2] Faculté des Sciences et Techniques Settat, B.P. 577, 26000 Settat, Maroc
[3] LPUB, CNRS, UMR 5027, Faculté des Sciences Mirande, 9 rue Alain Savary, B.P. 47870, 21078 Dijon Cedex, France
[4] Anorganische Chemie, FB C, Universität-GH, Gauss-str. 20, 42097 Wuppertal, Germany

Received 10 August 2004
Published online 30 November 2004

Abstract. Monoisotopic stannane $^{116}SnH_4$ has been investigated at room temperature in the 600–850 cm^{-1} and 1270–1600 cm^{-1} regions by FTIR spectroscopy with an effective resolution of 2.1×10^{-3} cm^{-1} and 2.0×10^{-3} cm^{-1} respectively. The simultaneous analysis of infrared transitions of both the bending triad and the hot band {bending triad} minus {bending dyad}, enabled us to determine 26 parameters for the $(2\nu_2)$ band and the combination band $(\nu_2+\nu_4)$. The standard deviation of the fit was about 1.5×10^{-3} cm^{-1}. In this analysis, we have used, for the bending triad, a Hamiltonian developed to the fourth order of approximation. 163 observed transitions for the hot band and most observed transitions for the bending triad spectrum, were assigned to the two bands $2\nu_2$ and $(\nu_2+\nu_4)$, up to $J=9$. In the fit of the Hamiltonian parameters, we have used for the ground state and for the fundamentals ν_2 and ν_4, the parameters determined by Brunet, Pierre, and Bürger [J. Mol. Spectrosc. **140**, 237 (1990)].

PACS. 33.20.Vq Vibration-rotation analysis – 33.20.Ea Infrared spectra

1 Introduction

The first vibration-rotation study of stannane SnH_4, was performed by Levin and Ziffer [2] who determined some spectroscopic constants and showed that the two bending modes ν_2 (E) and ν_4 (F_2) are strongly coupled by a first order Coriolis interaction. This kind of interaction is observed for all tetrahydride molecules XH_4 like CH_4 [3], CD_4 [4,5] and SiH_4 [6]. Kattenberg and Oskam [7] measured the four fundamental bands using Raman and infrared (IR) spectroscopies.

The first high-resolution study of natural stannane was performed by Ohshima et al. [8,9]. Their experimental technique used IR-microwave (MW) double resonance employing a tuneable diode laser which allowed them to observe three different types of transitions: rotational transitions in the ground state [8] and in the ν_2/ν_4 dyad excited states [9], and rovibrational transitions of the ν_2 and ν_4 bands between 640 and 850 cm^{-1}. Thereafter, Brunet et al. [1] made an analysis of the bending dyad (ν_2/ν_4) of monoisotopic stannane $^{116}SnH_4$ based on FTIR high-resolution spectra. The very high precision of the experimental IR spectrum and the very high accuracy of the model used in the analysis enabled them to determine simultaneously both ground and upper state parameters of the Hamiltonian developed to the sixth order approximation in the Amat-Nielsen classification.

The stretching modes ν_1 and ν_3 were investigated, too, by many authors. Birss [10] showed that the ν_1 and the ν_3 vibrational states are coupled by a second order rotation-vibration interaction term. This interaction is generally not strong but becomes very important when the wave number difference of the two interacting states is within a few reciprocal centimeters. In the IR, the formally forbidden ν_1 transitions can therefore be observed. Such interactions have been observed in SiH_4 [11] and GeH_4 [12]. Jörissen et al. [13] have recorded and analysed the IR spectrum of the (ν_1/ν_3) dyad of stannane in natural isotopic abundance. Their technique used IR-MW double resonance employing a tuneable diode laser. They have determined 17 constants for each of the five most abundant isotopic species of stannane by fitting simultaneously the IR and MW data. They have used for the ground state, the parameters determined by Ohshima et al. [8,9]. The Hamiltonian employed for the ground state and the $v_1=1$ was that of Kirschner and Watson [14] and that for the state $v_3=1$ as given by Robiette [15]. Only one coupling term between ν_1 and ν_3 given by Susskind in a tensorial form [16] was taken into account.

[a] e-mail: atabyaoui@yahoo.fr

Krivtsun et al. [17] made an analysis of the FTIR spectrum of $^{120}SnH_4$ in the 1903–1960 cm^{-1} region. More than 230 transitions were used to analyse the ν_1 and ν_3 resonance states. These authors have determined 21 spectroscopic parameters of the upper states using a Hamiltonian developed to the fourth order of approximation, which explicitly takes into account the resonance interactions.

Tabyaoui et al. [18,19] have recorded and analysed the FTIR and high-resolution stimulated Raman spectra of monoisotopic stannane, $^{116}SnH_4$. A simultaneous analysis of IR, Raman and MW [13,20] data with a Hamiltonian developed to sixth order for the (ν_1/ν_3) dyad enabled them to determine 4 parameters of ν_1, 17 parameters of ν_3, and 6 interaction parameters. Transitions were assigned up to $J = 14$. For high J values ($J > 14$), they have shown that the (ν_1/ν_3) dyad interacts with the bending tetrad $(v_1v_2v_3v_4) = (3\nu_2,\ 2\nu_2 + \nu_4,\ \nu_2 + 2\nu_4,\ 3\nu_4)$, as the third harmonic of the bending modes ν_2 and ν_4 is close to the stretching dyad (ν_1/ν_3). So, in order to analyse completely the IR spectrum of $^{116}SnH_4$ in the 1900 cm^{-1} region, the authors [18] propose that the full (ν_1, ν_3, $3\nu_2$, $2\nu_2 + \nu_4$, ν_2+$2\nu_4$, $3\nu_4$) polyad interaction scheme must be considered. That needs the good knowledge of the bending triad ($2\nu_2$, $\nu_2 + \nu_4$, $2\nu_4$) and the bending tetrad ($3\nu_2$, $2\nu_2 + \nu_4$, $\nu_2 + 2\nu_4$, $3\nu_4$) levels.

The present work is a first step toward this aim. It consists of an analysis of the bending triad ($2\nu_2$, $\nu_2 + \nu_4$, $2\nu_4$) of $^{116}SnH_4$ in the 1400 cm^{-1} region, based on high-resolution Fourier transform spectra. Moreover, use was made of hot band {bending triad} minus {bending dyad} transitions [21] occurring in the region of the bending dyad and reaching the triad levels in their upper states. The high precision of the experimental spectra and the high accuracy of the Hamiltonian model used in the analysis made it possible to determine 26 parameters corresponding to the $(2\nu_2)$ and $(\nu_2 + \nu_4)$ bands.

Transitions were assigned up to $J = 9$.

2 Experimental details

Monoisotopic stannane, $^{116}SnH_4$, was prepared by reacting a solution containing $SnCl_6^{2-}$ (1 mg Sn/ml), obtained by dissolving ^{116}Sn (98% ^{116}Sn, Oak Ridge) in an aqueous HCl/HNO_3 mixture, with an aqueous solution of $NaBH_4$ (3%) in vacuum (50−80 mbar). Gaseous $^{116}SnH_4$ evolved was collected at −196 °C and purified by repeated fractional condensation using a standard vacuumline, yield ∼90%.

The FTIR spectra of $^{116}SnH_4$ were recorded at Giessen, Germany, in the 600−850 cm^{-1} and 1250−1600 cm^{-1} range at room temperature with a Bruker 120 HR spectrometer equipped with a Ge/KBr beam splitter. A Globar source was employed, and a liquid He cooled Cu:Ge and MCT800 detector were used, respectively. For the two spectra, pressures of 1 mbar and 7 mbar and cells measuring 18.7 cm and 1.5 m respectively, were used. The effective line widths of weak lines (FWHM) were 2.1×10^{-3} cm^{-1} and 2×10^{-3} cm^{-1} respectively. The resolution based on maximum optical path difference was 2.3×10^{-3} cm^{-1} and 2.2×10^{-3} cm^{-1}, respectively. Trapezoidal apodization was employed. Calibration of the former spectrum was done with N_2O lines, reference [22], while H_2O lines [22] were used to calibrate the latter spectrum. Wave number accuracy is better than 1×10^{-3} cm^{-1}.

3 Theorical section

The transformed vibrational-rotational Hamiltonian for tetrahedral molecules developed by Champion and Pierre [23–25] is especially well adapted for vibrational extrapolation. Vibrational operators are expressed in terms of tensor products of creation and annihilation elementary operators in such a way that each term of the Hamiltonian expansion corresponds to a given vibrational state or set of quasi-degenerate vibrational states. According to this scheme, the completely transformed Hamiltonian for the vibrational states taken into account in this work, can be written as

$$\tilde{\mathbf{H}} = \tilde{\mathbf{H}}_{\{GS\}} + \sum_s \tilde{\mathbf{H}}_{\{\nu_s\}} + \sum_s \tilde{\mathbf{H}}_{\{2\nu_s\}} + \sum_{s<s'} \tilde{\mathbf{H}}_{\{\nu_s+\nu_{s'}\}} + ... \tag{1}$$

In this expansion, $\tilde{\mathbf{H}}_{\{GS\}}$ contains only pure rotational operators of the type J^Ω (J designating one component J_x, J_y or J_z of the angular-momentum operator). In the notation introduced in [23–25], its tensorial expression is

$$\tilde{\mathbf{H}}_{\{GS\}} = \sum \mathbf{t}_0^{\Omega(K,A_1)} \mathbf{T}_0^{\Omega(K,A_1)} \tag{2}$$

$\tilde{\mathbf{H}}_{\{\nu_s\}}$ gathers all terms of type $r_s^2 J^\Omega$ (r_s designating q_s or p_s) quadratic in the ν_s mode elementary operators. Its tensorial expression [23–25] is

$$\tilde{\mathbf{H}}_{\{\nu_s\}} = \sum \mathbf{t}_{s,s}^{\Omega(K,\Gamma)} \mathbf{T}_{s,s}^{\Omega(K,\Gamma)} \tag{3}$$

$\tilde{\mathbf{H}}_{\{\nu_s+\nu_{s'}\}}$ gathers all term quartic in the ν_s and $\nu_{s'}$ mode elementary operators of the type $r_s^2 r_{s'}^2 J^\Omega$. Its tensorial expression [23–25] is

$$\tilde{\mathbf{H}}_{\{\nu_s+\nu_{s'}\}} = \sum \mathbf{t}_{ss',ss'}^{\Omega(K,\Gamma)\Gamma_1\Gamma_2} \mathbf{T}_{ss',ss'}^{\Omega(K,\Gamma)\Gamma_1\Gamma_2}. \tag{4}$$

The expression for $\tilde{\mathbf{H}}_{\{2\nu_s\}}$ is quite similar and can be obtained by setting $s' = s$ in equation (4).

In the above expressions and throughout this paper, $\mathbf{T}_{s...,s'...}^{\Omega(K,\Gamma)\Gamma_1\Gamma_2}$ is a rovibrational operator obtained by coupling rotational and vibrational operators:

$$\mathbf{T}_{s...,s'...}^{\Omega(K,\Gamma)\Gamma_1\Gamma_2} = \beta_{\Omega K}^{\Gamma_1} (\mathbf{R}^{\Omega(K,\Gamma)} \times \mathbf{V}_{s...,s'...}^{\Gamma_1\Gamma_2(\Gamma)})^{(A_1)} \tag{5}$$

where

$$\begin{aligned} \beta_{\Omega K}^{\Gamma_1} &= 1 && \text{if } K \neq 0 \\ &= \sqrt{\Gamma_1} \left(\frac{-\sqrt{3}}{4} \right)^{(\Omega/2)} && \text{if } K = 0. \end{aligned}$$

The rotational operator $\mathbf{R}^{\Omega(K,\Gamma)}$ is obtained by tensorial coupling of elementary rotational operator Ω, and the vibrational operator $\mathbf{V}^{\Gamma_1\Gamma_2(\Gamma)}_{s\ldots,s'\ldots}$ is obtained by tensorial coupling of $s\ldots$ elementary creation operators and of $s'\ldots$ elementary annihilation operators. The value of $[\Gamma_1]$ is the dimension of the representation. Details of the coupling of different operators can be obtained in [25].

The rovibrational effective Hamiltonian for a set of interacting states $\langle v\rangle$ is given by:

$$\mathbf{H}^{\langle v\rangle} = \mathbf{P}^{\langle v\rangle}\tilde{\mathbf{H}}\mathbf{P}^{\langle v\rangle} \tag{6}$$

where $\mathbf{P}^{\langle v\rangle}$ is the projector operator on the vibrational Hilbert subspace.

The ground-state effective Hamiltonian contains terms from $\tilde{\mathbf{H}}_{\{GS\}}$ only:

$$\begin{aligned}\mathbf{H}^{\langle GS\rangle} &= \mathbf{P}^{\langle GS\rangle}\tilde{\mathbf{H}}_{\{GS\}}\mathbf{P}^{\langle GS\rangle}\\ &= \sum \mathbf{t}_0^{\Omega(K,A_1)}\mathbf{P}^{\langle GS\rangle}\mathbf{T}_0^{\Omega(K,A_1)}\ \mathbf{P}^{\langle GS\rangle}\end{aligned} \tag{7}$$

where $\mathbf{P}^{\langle GS\rangle}\mathbf{T}_0^{\Omega(K,A_1)}\mathbf{P}^{\langle GS\rangle}$ denotes the projection of the operator $\mathbf{T}_0^{\Omega(K,A_1)}$. For simplicity, in all subsequent formulae, the same symbol will be used for one operator and its projections in all Hilbert subspaces. For instance, (7) will be rewritten as

$$\mathbf{H}^{\langle GS\rangle} = \sum \mathbf{t}_0^{\Omega(K,A_1)}\mathbf{T}_0^{\Omega(K,A_1)} \tag{8}$$

Its matrix representation can be denoted by $\mathbf{H}^{\langle GS\rangle} = \mathbf{H}^{\langle GS\rangle}_{\{GS\}}$.

The effective Hamiltonian for the fundamental state $\langle\nu_s\rangle \equiv \{v_s = 1\}$ contains terms from $\tilde{\mathbf{H}}_{\{GS\}}$ and $\tilde{\mathbf{H}}_{\{\nu_s\}}$ only:

$$\begin{aligned}\mathbf{H}^{\langle\nu_s\rangle} &= \mathbf{P}^{\langle\nu_s\rangle}\left(\tilde{\mathbf{H}}_{\{GS\}} + \tilde{\mathbf{H}}_{\{\nu_s\}}\right)\mathbf{P}^{\langle\nu_s\rangle}\\ &= \sum \mathbf{t}_0^{\Omega(K,A_1)}\mathbf{T}_0^{\Omega(K,A_1)} + \sum \mathbf{t}_{s,s}^{\Omega(K,\Gamma)}\mathbf{T}_{s,s}^{\Omega(K,\Gamma)}.\end{aligned} \tag{9}$$

Its matrix representation can be expressed as the sum of two terms:

$$\mathbf{H}^{\langle\nu_s\rangle} = \mathbf{H}^{\langle\nu_s\rangle}_{\{GS\}} + \mathbf{H}^{\langle\nu_s\rangle}_{\{\nu_s\}}. \tag{10}$$

The effective Hamiltonian for the combination state $\langle\nu_s + \nu_{s'}\rangle \equiv \{v_s = v_{s'} = 1\}$ contains terms from $\tilde{\mathbf{H}}_{\{GS\}}$, $\tilde{\mathbf{H}}_{\{\nu_s\}}$, $\tilde{\mathbf{H}}_{\{\nu_{s'}\}}$ and $\tilde{\mathbf{H}}_{\{\nu_s+\nu_{s'}\}}$ only:

$$\begin{aligned}\mathbf{H}^{\langle\nu_s+\nu_{s'}\rangle} &= \mathbf{P}^{\langle\nu_s+\nu_{s'}\rangle}\big(\tilde{\mathbf{H}}_{\{GS\}} + \tilde{\mathbf{H}}_{\{\nu_s\}} + \tilde{\mathbf{H}}_{\{\nu_{s'}\}}\\ &\quad + \tilde{\mathbf{H}}_{\{\nu_s+\nu_{s'}\}}\big)\mathbf{P}^{\langle\nu_s+\nu_{s'}\rangle}\\ &= \sum \mathbf{t}_0^{\Omega(K,A_1)}\mathbf{T}_0^{\Omega(K,A_1)} + \sum \mathbf{t}_{s,s}^{\Omega(K,\Gamma)}\mathbf{T}_{s,s}^{\Omega(K,\Gamma)}\\ &\quad + \sum \mathbf{t}_{s',s'}^{\Omega(K,\Gamma)}\mathbf{T}_{s',s'}^{\Omega(K,\Gamma)}\\ &\quad + \sum \mathbf{t}_{s,s'}^{\Omega(K,\Gamma)\Gamma_1\Gamma_2}\mathbf{T}_{s,s'}^{\Omega(K,\Gamma)\Gamma_1\Gamma_2}.\end{aligned} \tag{11}$$

Its matrix representation can be expressed as sum of four terms:

$$\mathbf{H}^{\langle\nu_s+\nu_{s'}\rangle} = \mathbf{H}^{\langle\nu_s+\nu_{s'}\rangle}_{\{GS\}} + \mathbf{H}^{\langle\nu_s+\nu_{s'}\rangle}_{\{\nu_s\}} + \mathbf{H}^{\langle\nu_s+\nu_{s'}\rangle}_{\{\nu_{s'}\}} + \mathbf{H}^{\langle\nu_s+\nu_{s'}\rangle}_{\{\nu_s+\nu_{s'}\}}. \tag{12}$$

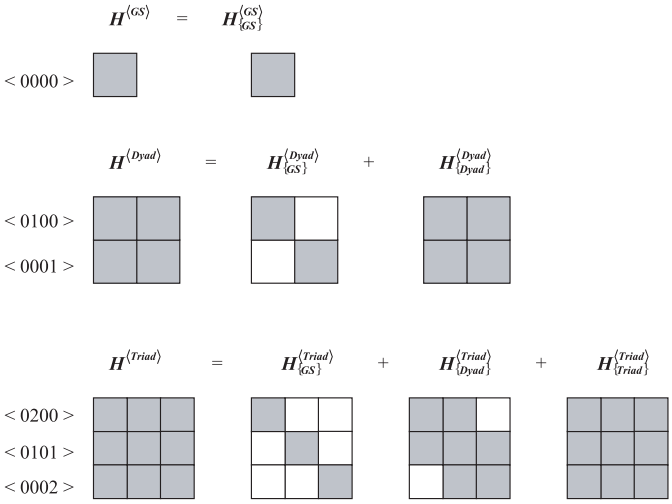

Fig. 1. Schematic presentations of effective Hamiltonian matrices.

The effective Hamiltonian for the harmonic state $\langle 2\nu_s\rangle \equiv \{v_s = 2\}$ is similarly obtained by setting $s = s'$ in the above expression. Its matrix representation can be expressed as a sum of three terms:

$$\mathbf{H}^{\langle 2\nu_s\rangle} = \mathbf{H}^{\langle 2\nu_s\rangle}_{\{GS\}} + \mathbf{H}^{\langle 2\nu_s\rangle}_{\{\nu_s\}} + \mathbf{H}^{\langle 2\nu_s\rangle}_{\{2\nu_s\}}. \tag{13}$$

In the general notation $\mathbf{H}^{\langle P\rangle}_{\{p\}}$, $\langle P\rangle$ specifies the Hilbert subspace (associated with the polyad P) on which H is operating, whereas $\{p\}$ specifies the type of the vibrational operators involved (relating to the polyad p). The v quantum numbers of the states included in polyad p are less or equal to that included in the polyad P. In practice, according to the so-called vibrational extrapolation scheme, the parameters involved in all subsequent effective Hamiltonians $\mathbf{H}^{\langle P\rangle}$ are those of the unique transformed Hamiltonian $\tilde{\mathbf{H}}$. In the cases considered in this work, three types of parameters can be distinguished:

$\mathbf{t}_0^{\Omega(K,A_1)}$	so-called ground-state parameters;
$\mathbf{t}_{s,s}^{\Omega(K,\Gamma)}$	so-called ν_s parameters;
$\mathbf{t}_{ss',ss'}^{\Omega(K,\Gamma)\Gamma_1\Gamma_2}$	so-called $(\nu_s + \nu_{s'})$ parameters (or $2\nu_s$ parameters if $s = s'$).

Figure 1 shows the Hamiltonian matrices in the three states considered here.

Perevalov et al. [26–29] showed that different unitary transformations of the effective Hamiltonian can be considered. These transformations change the eigenfunctions of the Hamiltonian but do not change its eigenvalues:

$$\tilde{\tilde{\mathbf{H}}} = e^{i\mathbf{S}}\tilde{\mathbf{H}}e^{-i\mathbf{S}} = \sum \tilde{\mathbf{t}}^{\Omega(K,n\Gamma)\Gamma_1\Gamma_2}_{s\ldots,s'\ldots} \times \mathbf{T}^{\Omega(K,n\Gamma)\Gamma_1\Gamma_2}_{s\ldots,s'..} \tag{14}$$

with

$$\mathbf{S} = \sum \mathbf{S}^{\Omega(K,n\Gamma)\Gamma_1\Gamma_2}_{s\ldots,s'\ldots}\left(\mathbf{R}^{\Omega(K,\Gamma)} \times {}^{\varepsilon}\mathbf{V}^{\Gamma_1\Gamma_2(\Gamma)}_{s\ldots,s'\ldots}\right)^{(A_1)}. \tag{15}$$

Table 1. Parameters of the $2\nu_2$ and $(\nu_2+\nu_4)$ bands of $^{116}SnH_4$.

$\Omega(K,n\Gamma)$	$s_1 s_2\ \Gamma_1 s_3 s_4\ \Gamma_2$	Value (cm^{-1})
0(0,0A1)	0200A1 0200A1	$-8.395(26)\times10^{-1}$
2(0,0A1)	0200A1 0200A1	$1.121(22)\times10^{-3}$
0(0,0A1)	0200 E 0200 E	1.32550(62)
2(0,0A1)	0200 E 0200 E	$-9.86(76)\times10^{-5}$
1(1,0F1)	2000A1 0101F1	$-4.237(24)\times10^{-2}$
1(1,0F1)	0200 E 0101F1	$4.060(28)\times10^{-2}$
1(1,0F1)	0200 E 0101F2	$-1.74(87)\times10^{-4}$
0(0,0A1)	0200A1 0002A1	$-3.17(55)\times10^{-2}$
2(0,0A1)	0200A1 0002A1	$6.17(66)\times10^{-4}$
0(0,0A1)	0200 E 0002 E	$4.71(34)\times10^{-2}$
2(0,0A1)	0200 E 0002 E	$-2.024(76)\times10^{-3}$
1(1,0F1)	0200 E 0002F2	$7.389(97)\times10^{-2}$
0(0,0A1)	0101F1 0101F1	2.30605(23)
1(1,0F1)	0101F1 0101F1	$-4.589(10)\times10^{-2}$
2(0,0A1)	0101F1 0101F1	$-1.1630(74)\times10^{-3}$
1(1,0F1)	0101F1 0101F2	$-1.24941(49)\times10^{-1}$
0(0,0A1)	0101F2 0101F2	$-7.6(1.1)\times10^{-4}$
1(1,0F1)	0101F2 0101F2	$-3.39699(73)\times10^{-1}$
2(0,0A1)	0101F2 0101F2	$-1.636(31)\times10^{-4}$
1(1,0F1)	0101F1 0002A1	$1.0544(49)\times10^{-1}$
1(1,0F1)	0101F1 0002 E	$-2.5247(51)\times10^{-1}$
1(1,0F1)	0101F1 0002F2	$-1.7923(41)\times10^{-1}$
1(1,0F1)	0101F2 0002 E	$-2.6628(47)\times10^{-1}$
0(0,0A1)	0101F2 0002F2	$-8.5484(47)\times10^{-1}$
1(1,0F1)	0101F2 0002F2	$1.4166(18)\times10^{-1}$
2(0,0A1)	0101F2 0002F2	$1.040(12)\times10^{-3}$

* One standard deviation in parenthesis.

These transformations keep the operator form and eigenvalues unalterated but change the values of its parameters, according to:

$$\tilde{\mathbf{t}} = \mathbf{t} + \Delta\mathbf{t}(\mathbf{s}^{(1)}, \mathbf{s}^{(2)}, ...) \tag{16}$$

Most of the $\mathbf{t}^{\Omega(K,n\Gamma)\Gamma_1\Gamma_2}_{s...,s'...}$ terms cannot be determined from observed lines in a unique way (for details, see Refs. [26–30]), they are not spectroscopic constants.

4 Data analysis

A new set of programs, grouped in a software package named STDS (Spherical Top Data System), was developed in the LPUB in Dijon [31]. These programs may be used to study the vibrational polyads with $J < 200$, they were adapted to refine at the same time several types of vibrational parameters that can belong to the ground state, dyad states, states connected by hot bands, etc.; by fitting simultaneously several types of experimental data. The whole package STDS is freely accessible through ftp (user anonymous) at `jupiter.u-bourgogne.fr` or through the World Wide Web site at `fttp://www.u-bourgogne.fr/LPUB/STDS.html`.

The analysis is based on an iterative weighted least-squares fitting procedure of the transition wave numbers. In order to minimize a dimensionless Q number in the least-squares procedure, the weight w_i for each piece of data f_i is equal to the inverse of the square of the estimated uncertainty Δ_i:

$$Q = \sum_i \frac{\left(f_i^{obs} - f_i^{cal}\right)^2}{\Delta_i^2}. \tag{17}$$

In practice, we assigned an uncertainty Δ_i of 1×10^{-3} cm^{-1} to unblended transitions for the bending triad and of 0.3×10^{-3} cm^{-1} for the hot band {bending triad} minus {bending dyad} transitions.

Of the 575 calculated transitions assigned to observed lines up to $J = 9$, 443 presumably unblended ones were used in the fit. IR data corresponding to the $2\nu_2$ and $(\nu_2+\nu_4)$ bands and to the hot band {bending triad} minus {bending dyad} [21] were combined to refine the Hamiltonian parameters. The ground state and the bending dyad (ν_2/ν_4) parameters used in the fit were fixed to the values determined by Brunet et al. [1]. Twenty-six parameters of the Hamiltonian, corresponding to the $2\nu_2$ and $(\nu_2+\nu_4)$ bands, were determined with a standard deviation of the fit of about 1.5×10^3 cm^1. The results are given in Table 1. Statistics of the fit are listed in Tables 2 and 3.

A graphical display of the quality of the present analysis is shown in Figure 2 in which the Obs-Cal residuals are plotted as a function of the wave number (a) and as a function of the rotational J number (b). This emphasizes the effect of neglected perturbations, which increases with J.

5 Rovibrational energy levels

The rovibrational energy levels are obtained by diagonalizing the effective Hamiltonian.

$$\mathbf{E}^{\langle\nu\rangle}(\mathbf{J},\mathbf{C},\alpha) = \langle\mathbf{J},\mathbf{C},\alpha|\,\mathbf{H}^{\langle\nu\rangle}\,|\mathbf{J},\mathbf{C},\alpha\rangle \tag{18}$$

where $|\mathbf{J},\mathbf{C},\alpha\rangle$ are the eigenfunctions of the effective rovibrational Hamiltonian, and α gives the energy levels of the vibrational polyads having the same J and C values.

Reduced energies are obtained by subtracting the scalar terms:

$$\mathbf{E}^{\langle\nu\rangle}_{red}(\mathbf{J},\mathbf{C},\alpha) = \mathbf{E}^{\langle\nu\rangle}(\mathbf{J},\mathbf{C},\alpha) - \sum_{\Omega}\mathbf{t}_0^{\Omega(0,0A_1)}(\mathbf{J}(\mathbf{J}+1))^{\Omega/2}. \tag{19}$$

Figure 3a shows all reduced calculated (0200) and (0101) levels up to $J = 9$ while Figure 3b shows the reduced energy levels reached by the observed transitions.

Table 2. Statistics on the fit of the infrared transitions of $^{116}SnH_4$. Bending triad.

28 Data for the (0200) band.

J	number of data	cumulated number of data	standard deviation (10^{-3} cm^{-1})	cumulated St. Dev. (10^{-3} cm^{-1})
6	4	4	1.127	1.127
7	9	13	0.964	1.017
8	11	24	1.012	1.015
9	4	28	0.724	0.978

280 Data for the (0101) band.

J	number of data	cumulated number of data	standard deviation (10^{-3} cm^{-1})	cumulated St. Dev. (10^{-3} cm^{-1})
0	1	1	1.157	1.157
1	7	8	0.853	0.897
2	15	23	0.775	0.819
3	20	43	1.008	0.912
4	30	73	0.822	0.876
5	38	111	0.796	0.850
6	39	150	0.735	0.822
7	52	202	0.969	0.862
8	44	246	0.869	0.863
9	34	280	0.962	0.876

Table 3. Statistics on the fit of the infrared transitions of $^{116}SnH_4$. Hot band {bending triad} minus {bending dyad} [21].

10 Data for the (0200) ← (0100) band.

J	number of data	cumulated number of data	standard deviation (10^{-3} cm^{-1})	cumulated St. Dev. (10^{-3} cm^{-1})
6	2	2	0.310	0.310
7	3	5	0.709	0.583
8	3	8	0.403	0.523
9	2	10	0.098	0.470

124 Data for the (0101) ← (0100) band.

J	number of data	cumulated number of data	standard deviation (10^{-3} cm^{-1})	cumulated St. Dev. (10^{-3} cm^{-1})
0	1	1	0.839	0.839
1	6	7	0.717	0.736
2	9	16	0.532	0.629
3	12	28	0.713	0.667
4	14	42	0.756	0.697
5	17	59	0.773	0.720
6	17	76	0.549	0.687
7	17	93	0.649	0.680
8	18	111	0.803	0.702
9	13	124	0.666	0.698

1 Data for the band (0101) ← (0001).

J	number of data	cumulated number of data	standard deviation (10^{-3} cm^{-1})	cumulated St. Dev. (10^{-3} cm^{-1})
7	1	1	0.244	0.244

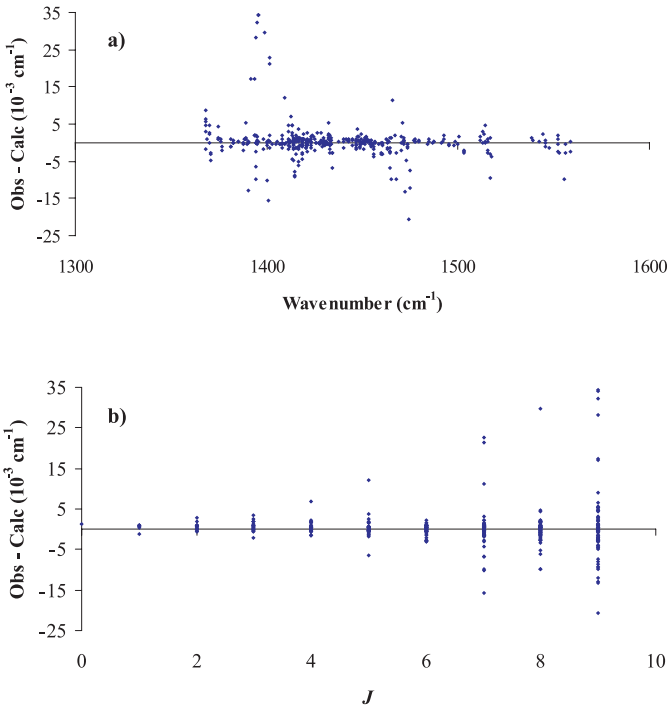

Fig. 2. Differences between experimental and calculated line positions: (a) as a function of the wave number; (b) as a function of the quantum number **J**.

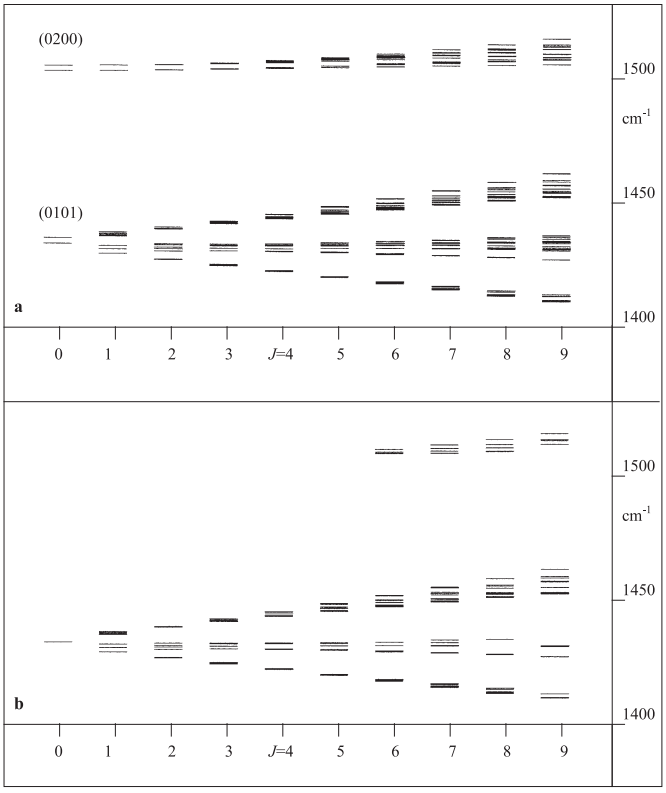

Fig. 3. Reduced energy level diagram: (a) All calculated levels. (b) Levels reached by the observed lines.

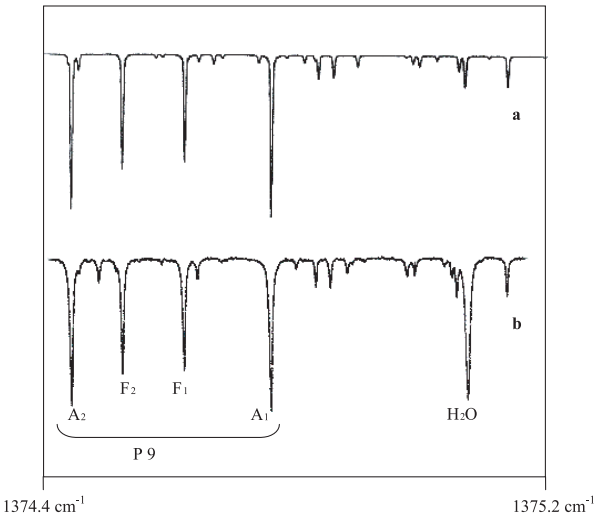

Fig. 4. Comparison of calculated (a) and experimental (b) spectra in the $(\nu_2 + \nu_4)$ P branch of $^{116}SnH_4$.

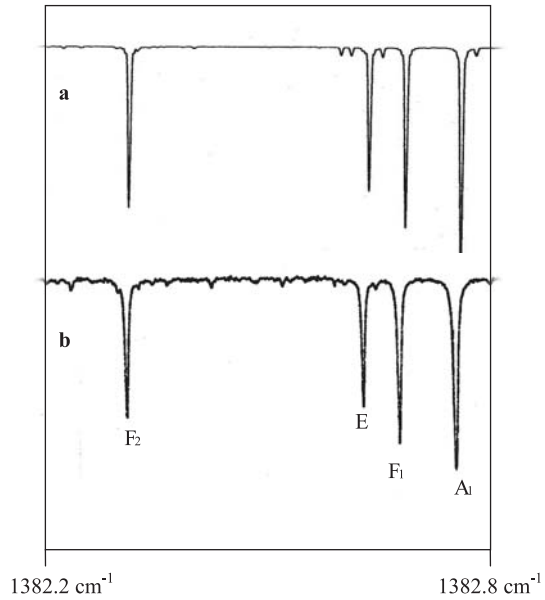

Fig. 5. Comparison of calculated (a) and experimental (b) spectra of P(8) in the $(\nu_2 + \nu_4)$ P branch of $^{116}SnH_4$.

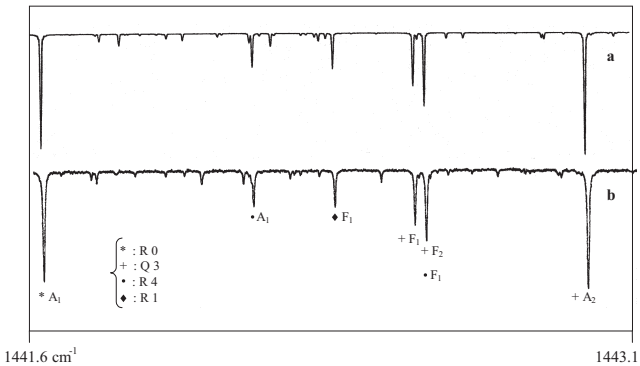

Fig. 6. Comparison of calculated (a) and observed (b) spectra in the $(\nu_2 + \nu_4)$ P branch of $^{116}SnH_4$.

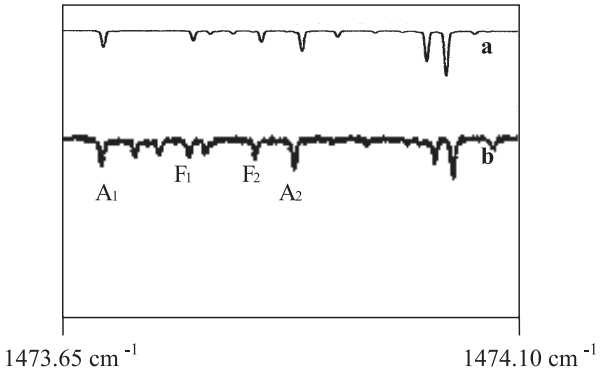

Fig. 7. Comparison of calculated (a) and observed (b) spectra of P(9) In the ($2\nu_2$) P branch of $^{116}SnH_4$.

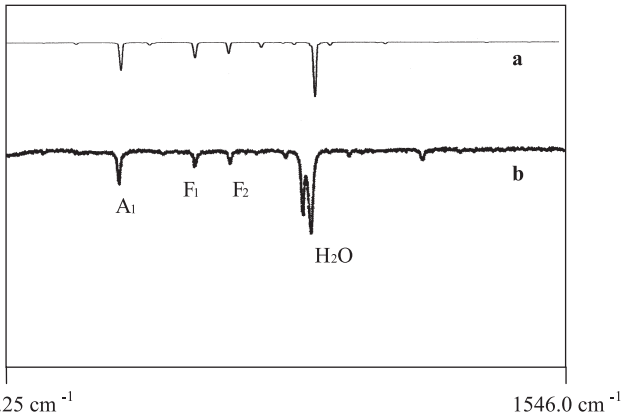

Fig. 8. Comparison of calculated (a) and observed (b) spectra of R(6) in the ($2\nu_2$) R branch of $^{116}SnH_4$.

6 Discussion

In the bending triad, the intensity of lines belonging to the $2\nu_4$ band is small. This made it so difficult to assign any transitions corresponding to the $2\nu_4$ band.

It is well-known that the $2\nu_2$, $(\nu_2 + \nu_4)$ and the $2\nu_4$ levels belonging to the bending triad are perturbed by resonance interactions. However, for relatively low values of J ($J < 10$) the isolated-state model is still applicable. With the aim to minimize the resonance interaction effect between the $(\nu_2 + \nu_4)$ and $2\nu_4$ bands, we analysed the infrared spectra up to $J = 9$.

Many lines corresponding to the $2\nu_2$ and $(\nu_2 + \nu_4)$ bands were assigned and a first set of the Hamiltonian parameters for these two bands has been determined. Altogether 163 transitions corresponding to the hot band {bending triad} minus {bending dyad} were assigned to observed lines with J up to $J = 9$ [21].

The calculated spectra are in excellent agreement with the experimental results (Figs. 4−9).

If we could use a double resonance technique to have a more intense and accurate spectrum in the 1100−1700 cm^{-1} region, we could probably reach levels that could help us to assign some $2\nu_4$ lines and complete the analysis for the full bending triad ($2\nu_2$, $\nu_2 + \nu_4$, $2\nu_4$).

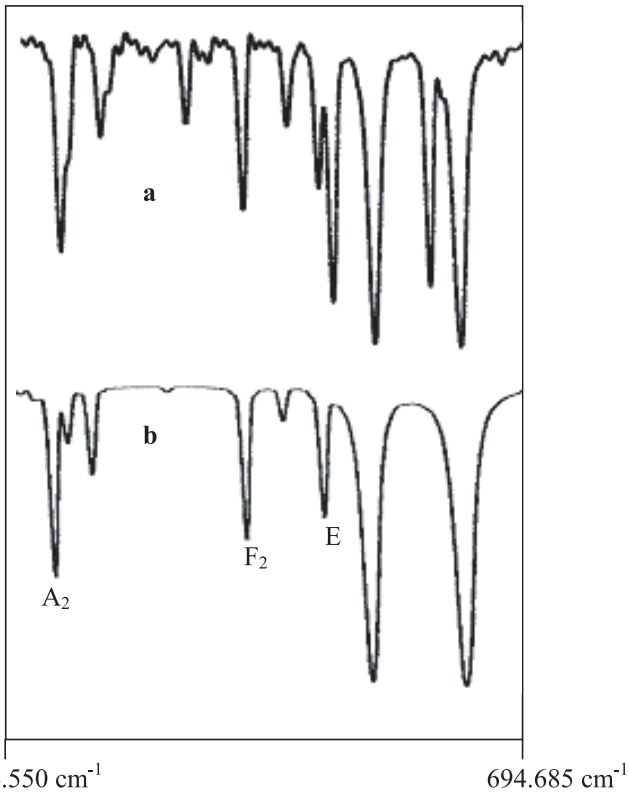

Fig. 9. Observed (a) and calculated (b) {bending triad} minus {bending dyad} hot band transitions of R(8) occurring in the bending dyad region of $^{116}SnH_4$.

We could then start the analysis of the bending tetrad ($3\nu_2$, $2\nu_2 + \nu_4$, $\nu_2 + 2\nu_4$, $3\nu_4$).

The author A. Tabyaoui would like to thank Ch. Wenger for his invaluable assistance. The "*Conseil Régional de Bourgogne*" is gratefully acknowledged for the financial support to the "*Laboratoire de Physique de l'Université de Bourgogne*".

References

1. F. Brunet, G. Pierre, H. Bürger, J. Mol. Spectrosc. **140**, 237 (1990)
2. I.W. Levin, H. Ziffer, J. Chem. Phys. **43**, 4023 (1965)
3. J.P. Champion et al., J. Mol. Spectrosc. **133**, 256 (1989)
4. M. Oldani et al., J. Mol. Spectrosc. **113**, 229 (1985)
5. G. Pierre et al., Can. J. Phys. **66**, 622 (1988)
6. G. Pierre, A. Valentin, L. Henry, Can. J. Phys. **64**, 341 (1986)
7. I.W. Kattenberg, A. Oskam, J. Mol. Spectrosc. **51**, 377 (1974)
8. Y. Ohshima et al., J. Chem. Phys. **85**, 5519 (1986)
9. Y. Ohshima et al., J. Chem. Phys. **87**, 5141 (1987)
10. F.W. Birss, Mol. Phys. **31**, 491 (1976)
11. A. Cabana et al., Mol. Phys. **36**, 1503 (1978)
12. P. Lepage, J.P. Champion, A.G. Robiette, J. Mol. Spectrosc. **89**, 440 (1981)
13. L. Jörissen et al., J. Chem. Phys. **90**, 2109 (1989)

14. S.M. Kirschner, J.K.G. Watson, J. Mol. Spectrosc. **47**, 347 (1973)
15. A.G. Robiette, D.L. Gray, F.W. Birss, Mol. Phys. **32**, 1591 (1976)
16. J. Susskind, J. Chem. Phys. **56**, 5152 (1972)
17. V.M. Krivtsun et al., J. Mol. Spectrosc. **139**, 107 (1990)
18. A. Tabyaoui et al., J. Mol. Spectrosc. **148**, 100 (1991)
19. A. Tabyaoui et al., Phys. Chem. News **10**, 106 (2003)
20. M. Takami, A. Tabyaoui, G. Pierre, in preparation
21. A. Tabyaoui, G. Pierre, H. Bürger, Eur. Phys. J. D **28**, 49 (2004)
22. G. Guelachvili, K. Narahari Rao, *Handbook of Infrared Standards* (Academic Press, San Diego, 1986)
23. J.P. Champion, Canad. J. Phys. **55**, 1802 (1977)
24. J.P. Champion, G. Pierre, J. Mol. Spectrosc. **79**, 255 (1980)
25. J.P. Champion, M. Loëte, G. Pierre, in *Spectroscopy of the earth's atmosphere and interstellar molecules*, edited by K.N. Rao, A. Weber (Academic Press, Inc. USA, 1992), p. 339
26. V.I. Perevalov, V.G. Tyuterev, B.I. Zhilinskii, Dokl. Acad. Nauk SSSR **263**, 868 (1982)
27. V.I. Perevalov, V.G. Tyuterev, B.I. Zhilinskii, J. Mol. Spectrosc. **103**, 147 (1984)
28. V.I. Perevalov, V.G. Tyuterev, B.I. Zhilinskii, Chem. Phys. Lett. **104**, 455 (1984)
29. V.I. Perevalov, V.G. Tyuterev, B.I. Zhilinskii, J. Mol. Spectrosc. **111**, 1 (1985)
30. C. Pierre, M. Loëte, G. Pierre, Can. J. Phys. **65**, 708 (1987)
31. M. Rey et al., J. Mol. Spectrosc. **219**, 313 (2003)